

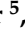



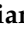






Article

Advancing Radiation-Detected Resonance Ionization towards Heavier Elements and More Exotic Nuclides

Jessica Warbinek ^{1,2,*} , Brankica Anđelić ^{1,3,4}, Michael Block ^{1,2,4} , Premaditya Chhetri ^{1,4}, Arno Claessens ⁵, Rafael Ferrer ⁵, Francesca Giacoppo ^{1,4} , Oliver Kaleja ^{1,6}, Tom Kieck ^{1,4} , EunKang Kim ², Mustapha Laatiaoui ² , Jeremy Lantis ², Andrew Mistry ^{1,7}, Danny Münzberg ^{1,2,4}, Steven Nothhelfer ^{1,2,4} , Sebastian Raeder ^{1,4} , Emmanuel Rey-Herme ⁸, Elisabeth Rickert ^{1,2,4}, Jekabs Romans ⁵ , Elisa Romero-Romero ² , Marine Vandebrouck ⁸, Piet Van Duppen ⁵  and Thomas Walther ⁹ 

- ¹ Abteilung Superschwere Elemente Physik, GSI Helmholtzzentrum für Schwerionenforschung, 64291 Darmstadt, Germany; andjelicbrankica@gmail.com (B.A.); m.block@gsi.de (M.B.); premaditya.chhetri@kuleuven.be (P.C.); f.giacoppo@gsi.de (F.G.); o.kaleja@gsi.de (O.K.); tomkieck@uni-mainz.de (T.K.); a.k.mistry@gsi.de (A.M.); dmuenzbe@students.uni-mainz.de (D.M.); nothhelfer@uni-mainz.de (S.N.); s.raeder@gsi.de (S.R.); e.rickert@uni-mainz.de (E.R.)
- ² Department Chemie—Standort TRIGA, Johannes Gutenberg-Universität Mainz, 55099 Mainz, Germany; eukim@uni-mainz.de (E.K.); mlaatiaoui@uni-mainz.de (M.L.); jlantis@uni-mainz.de (J.L.); eromeror@uni-mainz.de (E.R.-R.)
- ³ Faculty of Science and Engineering, University of Groningen, 9747 AG Groningen, The Netherlands
- ⁴ Sektion Superschwere Elemente Physik, Helmholtz Institut Mainz, 55099 Mainz, Germany
- ⁵ Department of Physics and Astronomy, KU Leuven, 3000 Leuven, Belgium; arno.claessens@kuleuven.be (A.C.); rafael.ferrer@kuleuven.be (R.F.); jekabs.romans@kuleuven.be (J.R.); piet.vanduppen@kuleuven.be (P.V.D.)
- ⁶ Institut für Physik, Universität Greifswald, 17489 Greifswald, Germany
- ⁷ Institut für Kernphysik, Technische Universität Darmstadt, 64289 Darmstadt, Germany
- ⁸ Irfu, CEA, Université Paris-Saclay, 91191 Gif-sur-Yvette, France; emmanuel.rey-herme@cea.fr (E.R.-H.); marine.vandebrouck@cea.fr (M.V.)
- ⁹ Institut für Angewandte Physik, Technische Universität Darmstadt, 64289 Darmstadt, Germany; thomas.walther@physik.tu-darmstadt.de
- * Correspondence: j.warbinek@gsi.de



Citation: Warbinek, J.; Anđelić, B.; Block, M.; Chhetri, P.; Claessens, A.; Ferrer, R.; Giacoppo, F.; Kaleja, O.; Kieck, T.; Kim, E.; et al. Advancing Radiation-Detected Resonance Ionization towards Heavier Elements and More Exotic Nuclides. *Atoms* **2022**, *10*, 41. <https://doi.org/10.3390/atoms10020041>

Academic Editor: Alexander Kramida

Received: 28 March 2022

Accepted: 13 April 2022

Published: 21 April 2022

Publisher's Note: MDPI stays neutral with regard to jurisdictional claims in published maps and institutional affiliations.



Copyright: © 2022 by the authors. Licensee MDPI, Basel, Switzerland. This article is an open access article distributed under the terms and conditions of the Creative Commons Attribution (CC BY) license (<https://creativecommons.org/licenses/by/4.0/>).

Abstract: Radiation-Detected Resonance Ionization Spectroscopy (RADRIS) is a versatile method for highly sensitive laser spectroscopy studies of the heaviest actinides. Most of these nuclides need to be produced at accelerator facilities in fusion-evaporation reactions and are studied immediately after their production and separation from the primary beam due to their short half-lives and low production rates of only a few atoms per second or less. Only recently, the first laser spectroscopic investigation of nobelium ($Z = 102$) was performed by applying the RADRIS technique in a buffer-gas-filled stopping cell at the GSI in Darmstadt, Germany. To expand this technique to other nobelium isotopes and for the search for atomic levels in the heaviest actinide element, lawrencium ($Z = 103$), the sensitivity of the RADRIS setup needed to be further improved. Therefore, a new movable double-detector setup was developed, which enhances the overall efficiency by approximately 65 % compared to the previously used single-detector setup. Further development work was performed to enable the study of longer-lived ($t_{1/2} > 1$ h) and shorter-lived nuclides ($t_{1/2} < 1$ s) with the RADRIS method. With a new rotatable multi-detector design, the long-lived isotope ^{254}Fm ($t_{1/2} = 3.2$ h) becomes within reach for laser spectroscopy. Upcoming experiments will also tackle the short-lived isotope ^{251}No ($t_{1/2} = 0.8$ s) by applying a newly implemented short RADRIS measurement cycle.

Keywords: laser spectroscopy; resonance ionization; atomic level scheme; gas cell; radiation detection; heavy actinides

1. Introduction

The study of the heaviest elements of the actinide series has recently gained much interest in the field of modern laser-based physics research [1]. Relativistic effects strongly influence the electronic configurations of these exotic elements, altering their atomic and chemical properties. Laser spectroscopy constitutes a powerful tool to study these effects, for example by measuring the ionization potential (IP) or by probing the atomic-level structure and optical transitions. Experimental data can benchmark theoretical predictions obtained through many-body methods such as relativistic coupled-cluster (RCC), the multi-configuration Dirac–Fock (MCDF), and the configuration interaction (CI) calculations [2]. In addition, laser spectroscopy can give access to nuclear structure observables, e.g., nuclear spin and nuclear moments or changes in the nuclear mean square charge radii, to validate and guide theoretical studies as for instance in the region of the heaviest elements around the $N = 152$ neutron shell closure [3].

To study these heavy elements, synthetic production of respective atoms is necessary as they do not naturally occur on earth. While the actinides up to fermium ($Z = 100$) can still be produced in macroscopic sample sizes from breeding processes in nuclear reactors [4], the transfermium elements ($Z > 100$) are exclusively produced in atom-at-a-time quantities in fusion-evaporation reactions at large-scale accelerator facilities. Therefore, measurements of their atomic properties are very challenging. Some of these properties can, for instance, be determined in gas- and liquid-phase chemistry experiments [5,6]. Only recently, the IPs of the heaviest actinides, ranging from fermium to lawrencium ($Z = 103$), were determined via a surface-ionization technique to meV precision [7,8]. However, the present accuracy of the IPs is limited by the applied technique, whereas the determination by laser spectroscopy can result in orders-of-magnitude higher precision. As of today, the heaviest element investigated by means of laser spectroscopy is the actinide element nobelium ($Z = 102$) [9]. The first ionization potential of this element was determined with a $50 \mu\text{eV}$ accuracy [10] to benchmark atomic theory and to probe relativistic effects on this property in the range of the heaviest elements.

The study of transfermium elements via common laser spectroscopy techniques such as collinear laser spectroscopy [11] or the hot-cavity technique [12] is often unfeasible. Due to the low production yield of only a few nuclei per second at most and the short half-lives, the application of laser spectroscopy requires a fast and extremely sensitive probing of the produced particles directly after their separation from the primary beam. The RADIATION-DETECTED RESONANCE IONIZATION SPECTROSCOPY (RADRIS) method [13,14] is dedicated to the study of exotic, heavy elements, and was successfully applied to find a ground-state transition in nobelium [9].

To date, an isotopic chain of nobelium isotopes ranging from mass numbers 252 to 254 has been investigated by this method [15]. For the study of short-lived nuclides with half-lives of $t_{1/2} < 1 \text{ s}$ such as the isotope ^{251}No ($t_{1/2} = 0.8 \text{ s}$), additional improvements are required due to significant decay losses expected in the measurement scheme. Further limitations appear for nuclides with half-lives of $t_{1/2} > 1 \text{ h}$. Moreover, a gain in the RADRIS efficiency could in general be decisive to identify resonance signals in future experiments such as for the search of yet experimentally undetermined atomic levels in elements heavier than nobelium.

Recent developments address these current limitations in terms of the range of accessible nuclides and the overall RADRIS efficiency. Here, the latest advances towards laser spectroscopy of longer-lived and shorter-lived transfermium nuclides are discussed, and corresponding results from on-line test experiments are presented. Additional development work towards an enhanced efficiency of RADRIS for the search for atomic levels in the heaviest actinide, lawrencium, will also be outlined.

2. Experimental Setup

2.1. RADRIS Technique

The RADRIS experimental setup consists of a stopping cell attached to the velocity filter SHIP at the GSI in Darmstadt [13,16]. A schematic drawing of the RADRIS setup is shown in Figure 1a. Recoil nuclei transmitted through the velocity filter enter the gas cell through an entrance window of 3.5 μm thin aluminum-coated mylar foil, supported by a stainless steel grid, and are stopped in 90 mbar argon buffer gas. A 1 mm \times 25 μm Hf-strip filament positioned opposite the entrance window and biased with an attractive voltage allows collecting incoming ions which adsorb and neutralize on the filament surface. By resistive pulse-heating of the filament, collected fusion products are re-evaporated to form a cloud of neutral atoms in the vicinity of the filament. Here, the evaporation temperature is critical for an efficient desorption paired with a minimum ion background from surface ionization processes. For an optimal filament choice, the IP of the collected atom species, the work function of the filament material, and the filament temperature are key parameters to be considered. A more detailed description of the desorption from filaments can be found in [17].

After the successful evaporation from the filament, the created neutral atoms are illuminated with two lasers following a two-step resonance ionization spectroscopy (RIS) scheme. Here, a UV-pumped dye laser supplies the first excitation step while the second, non-resonant step for ionization is provided by a high-power excimer or Nd:YAG laser. Resulting laser ions are then guided via suitable electric fields towards the detection area where they are collected on a 200 nm thin aluminized kapton foil in front of a Passivated Implanted Planar Silicon (PIPS) detector. Finally, the laser-ionized fusion products are detected via their alpha-decay energy. In this way, registered signals can additionally be gated by their characteristic decay energy to discriminate contributions of decay signals from background ions and subsequent decays of daughter nuclides.

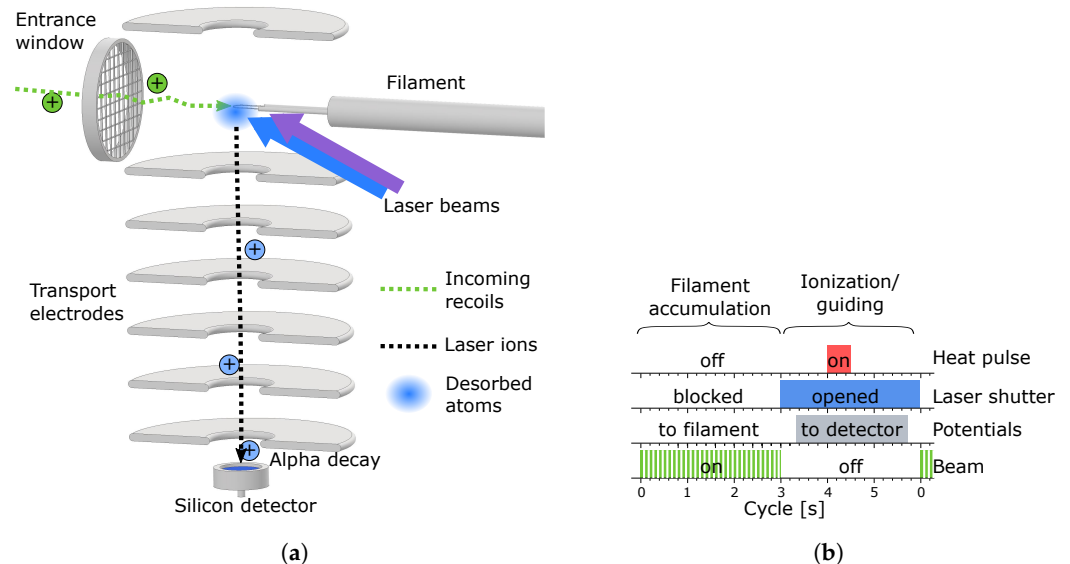


Figure 1. (a) Schematic drawing of the RADRIS setup. Incoming fusion products (green) enter the gas cell through the entrance window and thermalize in the 90 mbar argon buffer-gas environment. The recoils are collected on a Hf-strip filament, where they adsorb and neutralize. After desorption by pulse-heating the filament, an atomic cloud (blue) is formed around the filament which is illuminated with two lasers following a two-step RIS scheme. Resulting laser ions (blue) are guided towards a silicon detector by applying suitable transport electrode potentials where they are detected via their characteristic alpha-decay energy. (b) Previously applied RADRIS cycle for resonance ionization spectroscopy of ^{155}Yb . Delays between blocking the beam and changing the potentials, as well as applying the filament heat-pulse, are chosen to allow settling down of the stopped recoil ions and complete switching of the voltages, respectively [13].

2.2. RADRIS Measurement Cycle

The application of the RADRIS technique is cyclic, where each cycle is divided into the filament accumulation mode and the ionization/guiding mode. In the accumulation mode, fusion products enter the gas cell and are collected on the filament by applying an attractive potential compared to the surrounding electrodes and the chamber itself [13]. After the accumulation is completed, the setup is switched to the ionization/guiding mode in which the incoming primary beam is stopped, the laser shutters are opened to expose the stopping volume to laser light, and the potentials are set such that the created laser ions are guided towards the silicon detector. To change between the two modes, electrostatic potentials applied to the chamber, the filament, and the transport electrodes surrounding the filament need to be switched by giving an analog trigger to the power supplies after the primary beam is stopped. A time of approximately 0.3 s is required for the potentials to reach the set values. After switching the potentials, the filament is pulse-heated to desorb collected fusion products followed by laser ionization. Before starting the next cycle and unblocking the primary beam, both laser shutters are closed and the potentials are switched back for the next accumulation on the filament.

To ensure an optimum duty cycle, the beam break in the cycle should be as short as possible. However, the exact timing of the potential switching in the cycle is crucial to prevent any direct transport of incoming, positively charged fusion products onto the detector creating a background count rate independent of any laser interaction. Therefore, a delay of 0.3 s between beam blocking and the potential switching is considered in the cycle. An additional delay of 0.7 s between the switch of the potentials and pulse-heating the filament ensures a completed change to the guiding mode before the filament has reached the desorption temperature towards the end of the heat pulse. A typical RADRIS cycle for resonance ionization of incoming ^{155}Yb fusion products ($t_{1/2} = 1.8$ s) is shown in Figure 1b. For this isotope, the cycle features an accumulation on the filament for the accelerator beam-on period of 3 s and a beam break of 3 s.

3. New Detector Developments

The total RADRIS efficiency, which corresponds to the ratio of detected laser ions and incoming fusion products, does not only depend on the transport efficiency and the detection efficiency, but also on the duty cycle due to the cyclic application of the RADRIS technique. In the current setup, the detection efficiency is limited to 40% due to the covered solid angle by the detector for alpha decay on the foil [13]. For short-lived nuclides and respective short cycles, additional losses due to radioactive decay reduce the overall efficiency and hamper the study of nuclides with half-lives $t_{1/2} < 1$ s. For long-lived nuclides on the other hand, longer beam breaks after a completed measurement point are necessary, reducing the duty cycle and efficient beamtime usage. Thus, the RADRIS cycle needs to be adapted for each isotope depending on its half-life [18]. New developments were initiated to improve the overall efficiency for the application of RADRIS to different nuclides.

3.1. Rotatable Detector Setup

In the previously used design of the RADRIS setup [13], each measurement point required a waiting time long enough to detect subsequent decays of resonantly ionized products collected on the detector. To allow for a more efficient usage of beamtime when longer-lived (>1 h) nuclides are studied, a rotatable multi-detector setup was developed. This setup enables to parallelize multiple measurements on long-lived nuclides by decoupling the collection phase on the detector from the measurements of subsequent alpha decays. The new design combines three identical PIPS detectors with an active area of 450 mm^2 on a rotatable feedthrough, as shown in the schematic drawing in Figure 2a. The three detectors are positioned such that one of these detectors is placed on-axis with the transport electrodes to collect generated laser ions (the collection mode), while the other detectors are positioned off-axis to register residual alpha activity on their surfaces (the detection mode). After the collection is concluded on the on-axis detector, the detector

setup is rotated such that the next detector is in the collection mode, now for laser ions produced by light of the excitation laser tuned to the next wavelength.

In this new setup, recoil ions are directly guided onto the detectors without an additional collection foil in front. In this way, the detection efficiency for each detector can be increased from 40% to 50%. The increased tailing in the alpha spectra due to the decay of collected nuclides on the detector surface itself does not impact alpha signals from decays that differ by more than 0.25 MeV, as can be seen in the spectrum in Figure 2a.

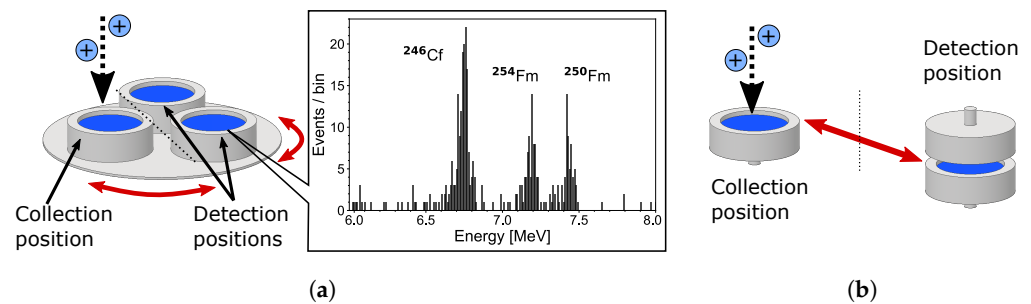


Figure 2. (a) Schematic drawing of the rotatable RADRIS detector setup. Laser ions (blue) are guided towards the PIPS detector in on-axis position in the collection mode. For the next collection, the detectors are rotated such that the next detector is placed on-axis with the chamber. Subsequent decays on the prior collection detector are registered in an off-axis detection position. An alpha spectrum on one of the detectors is shown for accumulated ^{254}Fm RIS signals of a measurement time of approximately 5 days. (b) Schematic drawing of the movable double-detector setup. Laser ions (blue) are guided towards the on-axis PIPS detector in the collection mode. For the detection mode, the detector is moved on top of a second PIPS detector to detect alphas emitted in the hemisphere opposite the active area of the collection detector.

The new detector arrangement was recently commissioned and tested in a first on-line laser spectroscopy of ^{254}Fm with a half-life of 3.2 h. These data are still under analysis and will be published independently. Figure 2a includes accumulated alpha spectra of the ^{254}Fm laser ions on one of the three detectors. With only a single detector, approximately one day per scan step of the excitation laser was expected to be required, while using the rotatable detector setup shortened the measurement time per detector and wavelength step to only seven hours. The resulting time gain allowed performing this experiment in 5.5 days with parasitic beam (5 ms long beam pulses with a repetition rate of 5 Hz) from the UNILAC accelerator at the GSI.

3.2. Movable Detector Setup

New challenges for the RADRIS technique arise when applying it to heavier and more exotic nuclei for which an enhancement in the overall efficiency can be of utmost importance. One of these challenges is the search for atomic levels in lawrencium, as for instance the production yield of ^{255}Lr (≈ 437 nb) is approximately one order of magnitude lower than for ^{254}No (≈ 2050 nb) [19,20] which was previously investigated for the search for atomic levels in nobelium [9]. In addition, predicted atomic levels accessible for laser spectroscopy range from 20,000 to 30,000 cm^{-1} [21–25], which would require an extended measurement time to identify a first atomic level. Thus, a combination of an enhancement in the sensitivity and efficiency of the detection method will benefit the search for atomic energy levels. To enhance the applicability of the RADRIS technique, a new setup with a movable detector was designed as shown in Figure 2b. This new detector system includes a double-PIPS detector setup, where both detectors have an active area of 600 mm^2 . The collection PIPS detector is placed on rails, enabling the movement of this detector between an on-axis position for laser ion collection and an off-axis position located on top of the second detector, where the active areas of both detectors face each other. The swap between both positions occurs via a fast pneumatically-coupled linear feedthrough with a 50 mm stroke in less than 1 s. During accumulation on the filament for a next wavelength step, the collection detector

is moved to rest on top of the second PIPS. The efficiency of detecting the alpha decay of collected nuclei is hence increased, as usually approximately 50% of the alphas emitted in the hemisphere opposite the active detector area would be lost. In this constellation, the second detector with a distance of approximately 4 mm between both active areas increases the rate of detected events. More than 65% of the fraction of alpha events seen by the collection detector can now be detected with the additional detector, which would usually be missed.

For future experiments on longer-lived species, the movable and rotatable detector designs can be combined by adding detectors opposite to those detectors in the detection mode on the rotatable setup.

4. Short RADRIS Cycle Development

With typical RADRIS cycles, laser spectroscopic investigations on short-lived nuclides ($t_{1/2} < 1$ s) are not feasible due to radioactive decay losses. Therefore, a new RADRIS cycle scheme for such nuclides was developed and applied to ^{154}Yb in recent on-line measurements. This isotope with a half-life of only $t_{1/2} = 0.4$ s and a relatively high production rate compared to the heavy actinides represents an ideal test case for the application of RADRIS to short-lived nuclei. This nuclide is produced in complete fusion-evaporation reactions of a ^{48}Ca beam at a beam energy of 4.55 MeV u^{-1} on a ^{112}Sn target in the $^{112}\text{Sn}(^{48}\text{Ca},6n)^{154}\text{Yb}$ reaction channel at the SHIP separator. Figure 3a shows the alpha-decay spectrum of produced nuclides in this reaction after direct transport to a single PIPS detector. In addition to ^{154}Yb , other isotopes such as $^{155,156}\text{Yb}$, and other radionuclides are present in the alpha spectrum as shown in Figure 3b, as different evaporation channels exist for the de-excitation of the compound nucleus $^{160}\text{Yb}^*$. In addition, decay daughters with significant alpha-branching ratios along the decay chains are present. As these nuclides from different evaporation channels have similar velocities, the velocity filter SHIP transports them to the focal plane. Thus, measured alpha-decay signals need to be carefully gated according to the respective alpha-decay energies for unambiguous identification.

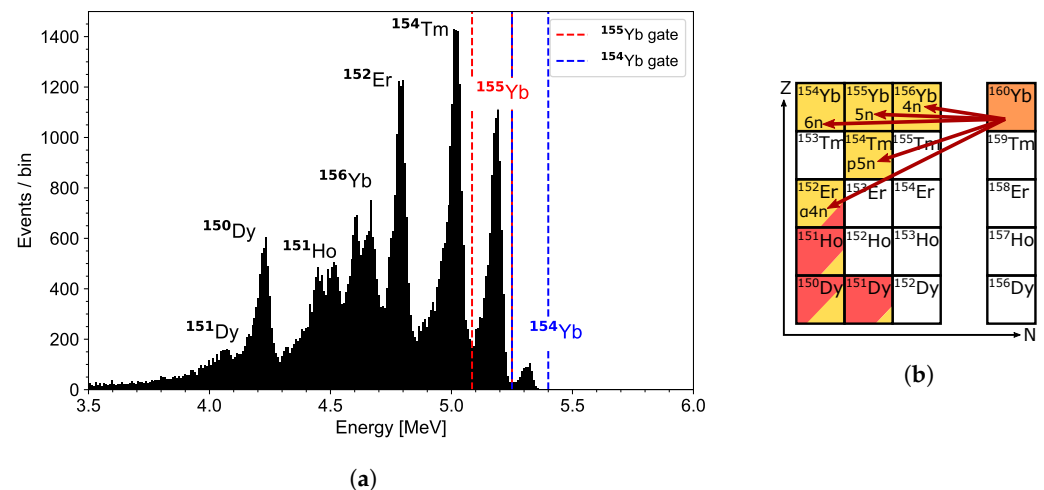


Figure 3. (a) Alpha spectrum of indirectly and directly produced nuclei in the $^{48}\text{Ca}+^{112}\text{Sn}$ fusion-evaporation reaction guided directly onto the PIPS detector after stopping inside of the gas cell. The signal strengths mostly reflect the respective production cross sections. Additionally, decay losses during ion transport through the gas cell impact the signal strength especially of the short-lived ^{154}Yb . Data for this spectrum were collected for 50 min with parasitic beam of 5 ms long beam pulses with a repetition rate of 5 Hz from the UNILAC accelerator at the GSI. (b) Observed evaporation channels of the $^{48}\text{Ca}+^{112}\text{Sn}$ fusion-evaporation reaction for a beam energy of 4.55 MeV u^{-1} . Shown are products and the subsequent daughter nuclides decaying via alpha decay which are mainly observed in the experiment.

To systematically understand the limitations of the cycles in terms of ion mobility in the gas cell, the transport time of ^{154}Yb through the cell to the detector was investigated. Therefore, reaction products were created during 5 ms long pulses of the UNILAC accelerator with a repetition rate of 1 Hz and entered the RADRIS gas cell, where they were stopped and transported directly to the detector. Figure 4a shows the time evolution of energy-gated and time-binned alpha events of ^{154}Yb as a function of the cycle time. Due to the limited mobility [6,26] of the Yb ions in the argon buffer gas, the ions reach the detector with a certain delay. The stopping distribution of the recoils in the gas cell [27] in addition to diffusion processes lead to an increased width of the distribution of the ions' arrival time at the detector. To determine the time required for the ions to reach the detector, one has to solve the differential equation describing the increasing number of ^{154}Yb ions on the detector after every accelerator beam pulse with respect to their successive decay as

$$\frac{dN}{dt} = A \cdot e^{-\frac{(t-t_c)^2}{2w^2}} - \lambda \cdot N,$$

and fit the obtained solution for $N(t)$ to the measured distribution in Figure 4a. Here, N describes the number of ions, A the amplitude of the distribution, t the cycle time, t_c the center of the time distribution, w its width, and $\lambda = \frac{\ln(2)}{t_{1/2}}$ the decay constant of ^{154}Yb . For this model, a Gaussian time distribution for the ions reaching the detector was assumed. The transport time, defined as the time required for 84.13% of the ions in the arrival-time distribution to reach the detector (corresponding to the centroid t_c of the distribution plus $1w$), was determined to be 0.33 s in argon buffer gas at a pressure of 90 mbar and a potential gradient of approximately 29 V/cm from the filament to ground potential on the detector.

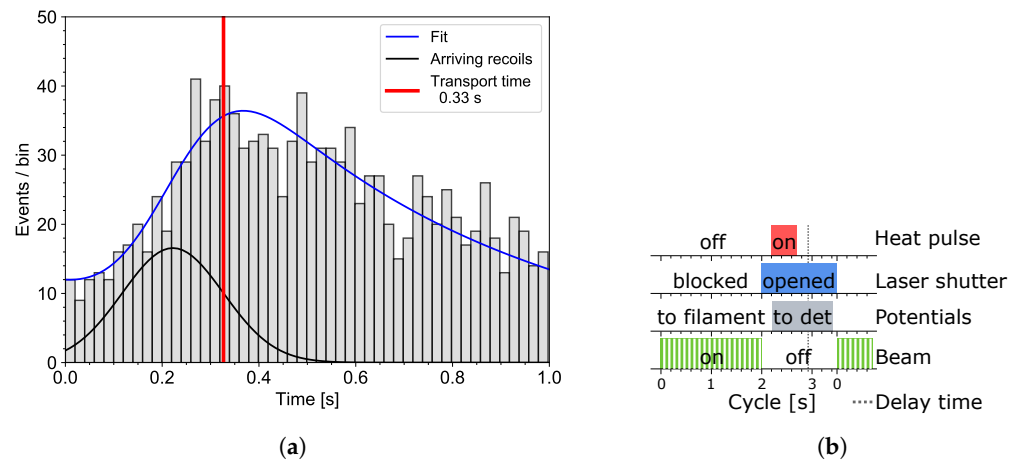


Figure 4. (a) Time structure of decay signals from incoming nuclei produced by 5 ms pulses from the accelerator with a repetition rate of 1 Hz. The incoming ions were directly transported to the detector. The transport time marked in red is determined as the time needed for 84.13% of the ions within the assumed Gaussian time distribution (black) to arrive on the detector. For more details, see text. (b) New, short RADRIS cycle for resonance ionization spectroscopy of ^{154}Yb . The overall cycle, as well as the beam break and the delay between beam stop and potential switch were generously shortened. The delay time between stopping of the accelerator beam and arrival of laser ions is marked in the cycle and needs to be considered for further decay losses.

Taking this boundary condition into account, a short RADRIS cycle as shown in Figure 4b was implemented. A simplified, faster configuration was tested in which only the filament potential is switched instead of switching the potential of multiple transport electrodes. To speed up the filament potential switching, a fast high-voltage switch (Behlke GHTS) was used, enabling a switching time of a few ms. With this rapid switching, the new, short RADRIS cycle features a waiting time between the potential switch and the pulse-heating of the filament reduced to 0.2 s to allow settling down of the stopped recoil

ions, thus reducing further decay losses. With this modification and the new potential configuration for ion accumulation on the filament, no additional losses in the ion transport were observed.

To determine the RADRIS efficiency with the short cycle, the short-lived ^{154}Yb was resonantly laser-ionized together with the neighboring, longer-lived ^{155}Yb . Hereby, the ratio of $^{154}\text{Yb}/^{155}\text{Yb}$ was measured to be $R = 7.40(16)\%$ in the focal plane [28] as can be seen also in the alpha spectrum in Figure 3a. For laser spectroscopy of both isotopes, a two-step RIS scheme as shown in Figure 5b was employed. A grating dye laser was deployed in broadband configuration with approximately 6 GHz linewidth for the first excitation step (FES). The second excitation step (SES) was provided by a high-power excimer laser. By discriminating the registered alpha-decay energies, laser-induced signals stemming from the two investigated Yb isotopes could be individually identified.

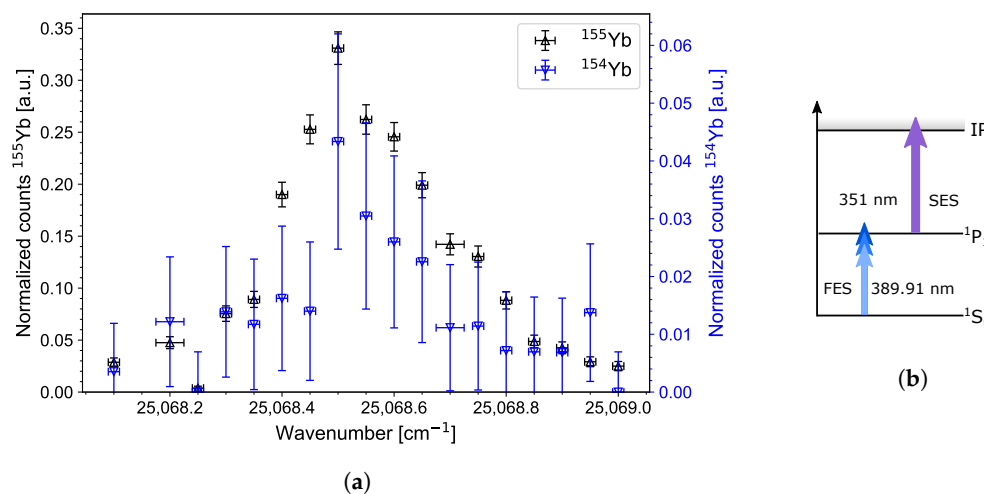


Figure 5. (a) Resonance ionization signal of ^{155}Yb (black) and ^{154}Yb (blue). Both rates are normalized to their respective count rates for a direct transport of produced recoil nuclei per accumulated charge integral of the primary beam. (b) RIS scheme for laser spectroscopy of $^{154,155}\text{Yb}$. The first excitation step was provided by a dye laser, the second, non-resonant step for ionization by a high-power excimer laser.

5. Results with the Short RADRIS Cycle Implementation

For characterization of the short cycle, results from laser spectroscopy of the short-lived ^{154}Yb isotope were compared with those obtained for ^{155}Yb , providing information on the RIS efficiency for ytterbium isotopes of different half-lives. The energy-gated alpha-decay signal in dependence of the wavenumber of the FES is shown in Figure 5a, and the applied RIS scheme is presented in Figure 5b. The RIS count rates of ^{154}Yb and ^{155}Yb were normalized to the primary-beam integral for comparison with the respective rate of guiding ions directly to the detector. With the short cycle, it was possible to detect ^{154}Yb from resonant laser ionization for the first time. The limited resolution in the gas cell [27] did not allow resolving the hyperfine structure of three expected hyperfine components in ^{155}Yb with a nuclear spin of $I = 7/2$. In addition, the expected isotope shift of around 1 GHz [29–32] is much smaller compared to the spectral linewidth of the FES laser of approximately 6 GHz and has therefore not been properly determined with the available statistics. Due to the large linewidth, the expected hyperfine splitting has not been observed to additionally contribute to the broadening of the resonance.

To determine the respective RIS efficiency, a Gaussian fit was applied to both isotope spectra to extract the maximum normalized count rate on resonance. From the ratio of the obtained RIS signal rate to the signal rate from direct transport to the detector, a half-life-dependent efficiency was determined, which is depicted in Figure 6 as black symbols. In addition to $^{154,155}\text{Yb}$, also the nuclides ^{254}No ($t_{1/2} = 51.2\text{ s}$) and ^{252}No ($t_{1/2} = 2.46\text{ s}$) were investigated with respect to RIS and direct transport count rates on the detector and

respective efficiencies added to the results in Figure 6. It has to be noted that for ^{252}No and ^{254}No different cycles, optimized for the respective half-lives, were applied.

To conclude if the experimentally determined efficiency dependence is fully governed by the expected decay losses and to exclude additional losses due to other effects, the total efficiency ϵ_{Cycle} of the different cycles was calculated analogously to [18]. Decay losses during accumulation on the filament and the overall usage of beamtime were considered by using the equation

$$\epsilon_{\text{Cycle}} = \frac{t_{1/2}}{(t_{\text{beam}} + t_{\text{break}}) \cdot \ln(2)} \left[1 - e^{-\frac{\ln(2)}{t_{1/2}} \cdot t_{\text{beam}}} \right] \cdot e^{-\frac{\ln(2)}{t_{1/2}} \cdot t_{\text{delay}}}$$

Here, $t_{1/2}$ is the half-life of the considered nuclide, t_{beam} (2 s in the case of the short cycle) is the beam-on time which equals the accumulation time on the filament, t_{break} (1.5 s for the short cycle) is the time of the beam break. For the calculation, a continuous production during the accumulation phase was assumed, followed by a decay of the collected population with the respective half-life. Additional losses during the beam break are considered by the last exponential function with $t_{\text{delay}} = 0.93$ s being the time between the beam shutoff and the ions reaching the detector in their required transport time after the desorption and resonant ionization. The calculated efficiencies for the respective cycles and nuclide half-lives are shown as red symbols in Figure 6. As the trend is of most importance in the comparison of experimental with calculated values, both values for ^{254}No were chosen to coincide in the graph. From the observed trend it becomes clear that the experimental behavior is fully described by decay losses. This enables forecasting the RADRIS performance for other exotic cases such as the isotope ^{251}No , for which a RIS-to-direct transport ratio of 0.053 was calculated for the new short cycle of 3.5 s duration with a break of 1.5 s shown in Figure 4b.

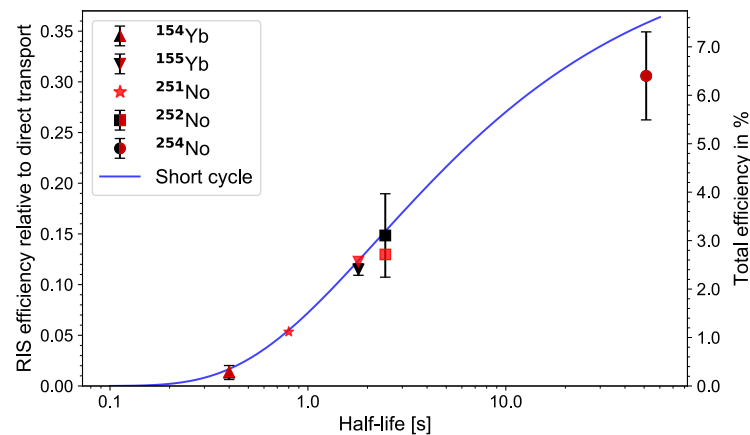


Figure 6. Comparison of efficiencies for rates of laser ions (with the laser frequency tuned on resonance) relative to direct transport rates. Experimentally determined efficiencies are shown in black. Red data points show estimated efficiencies of the RADRIS cycles in relation to the experimental RIS efficiency of ^{254}No . Overall efficiencies of the RADRIS setup are added with the right scale considering the known efficiency for ^{254}No [9].

From previous experiments on ^{254}No and ^{252}No , the total efficiency of the setup is known as number of detected laser ions in resonance relative to the number of respective recoil ions in the focal plane. The overall efficiencies were previously determined to $6.4\% \pm 1.0\%$ and $3.3\% \pm 1.0\%$ for ^{254}No and ^{252}No , respectively [9]. Comparing the expectation values for ^{251}No to ^{254}No , a total efficiency of 1.1% is expected for the performance of the setup with the short cycle. For a future RADRIS experiment on the nobelium isotope ^{251}No , with a production cross section of 30 nb [19], a RIS signal rate of approximately 2.5 ions per hour can be expected.

6. Conclusions and Outlook

Different aspects in improving the performance of the RADRIS technique were investigated in this work. A new rotatable detector assembly was successfully commissioned, extending the half-life range of nuclides accessible by RADRIS to half-lives of at least 3 h. With the newly implemented short RADRIS cycle, short-lived nuclides with half-lives of less than 1 s can now be studied, which was demonstrated on the short-lived isotope ^{154}Yb with $t_{1/2} = 0.4$ s. From comparison with calculations, the expected efficiency for the application of this new cycle to ^{251}No is sufficient to allow the first optical spectroscopy of this isotope. Further upcoming experiments will focus on the search for atomic levels in lawrencium, for which the newly developed movable double-detector design features an efficiency gain with the second detector giving a decisive benefit. For future experiments, a re-designed transport electrode structure in combination with the double-detector setup will soon be commissioned in the upcoming beamtimes at the GSI to further boost the overall efficiency of the RADRIS technique.

Author Contributions: Conceptualization, J.W., B.A., M.B., P.C., A.C., R.F., F.G., O.K., T.K., E.K., M.L., J.L., A.M., D.M., S.N., S.R., E.R.-H., E.R., J.R., E.R.-R., M.V., P.V.D. and T.W.; methodology, J.W., M.B., P.C., T.K., M.L. and S.R.; investigation, J.W., B.A., M.B., P.C., R.F., F.G., O.K., E.K., M.L., J.L., D.M., S.N., S.R., E.R.-H., E.R. and E.R.-R.; software, P.C.; formal analysis, J.W. and S.R.; data curation, J.W. and S.R.; writing—original draft preparation, J.W.; writing—review and editing, M.B. and S.R.; visualization, J.W.; supervision, M.B. and S.R.; project administration, M.B. and S.R.; funding acquisition, M.B., P.V.D. and T.W. All authors have read and agreed to the published version of the manuscript.

Funding: This work has been supported by the Bundesministerium für Bildung und Forschung (BMBF, Germany) under Project No. 05P18UMCIA. This project has received funding from the European Union’s Horizon 2020 research and innovation programme under grant agreement No 861198–LISA–H2020–MSCA–ITN–2019. E.K., E.R.-R. and M.L. acknowledge funding from the European Research Council (ERC) under the European Union’s Horizon 2020 Research and Innovation Programme (Grant Agreement No. 819957). P.V.D., A.C., R.F. and J.R. acknowledge funding from the Research Foundation – Flanders (FWO) and from the EOS (nr. 30468642) project of the FWO and F.R.S.-FNRS under the Excellence of Science (EOS) programme. T.W. acknowledges funding from the Bundesministerium für Bildung und Forschung (BMBF, Germany) under grant number 05P21RDFN1.

Data Availability Statement: The data presented in this study are available on request from the corresponding author.

Conflicts of Interest: The authors declare no conflict of interest.

Abbreviations

The following abbreviations are used in this manuscript:

RADRIS	RAAdiation-DeTected Resonance Ionization Spectroscopy
IP	Ionization Potential
RCC	Relativistic Coupled-Cluster
MCDF	Multi-Configuration Dirac-Fock
CI	Configuration Interaction
SHIP	Separator for Heavy Ion reaction Products
UNILAC	Universal Linear Accelerator
UV	Ultraviolet
SES	Second Excitation Step
FES	First Excitation Step
RIS	Resonance Ionization Spectroscopy
PIPS	Passivated Implanted Planar Silicon

References

1. Block, M.; Laatiaoui, M.; Raeder, S. Recent progress in laser spectroscopy of the actinides. *Prog. Part. Nucl. Phys.* **2021**, *116*, 103834.
2. Eliav, E.; Fritzsche, S.; Kaldor, U. Electronic structure theory of the superheavy elements. *Nucl. Phys. A* **2015**, *944*, 518–550.
3. Campbell, P.; Moore, I.; Pearson, M. Laser spectroscopy for nuclear structure physics. *Prog. Part. Nucl. Phys.* **2016**, *86*, 127–180.
4. Robinson, S.M.; Benker, D.E.; Collins, E.D.; Ezold, J.G.; Garrison, J.R.; Hogle, S.L. Production of Cf-252 and other transplutonium isotopes at Oak Ridge National Laboratory. *Radiochim. Acta* **2020**, *108*, 737–746.
5. Schädel, M.; Shaughnessy, D. *The Chemistry of Superheavy Elements*; Springer: Berlin/Heidelberg, Germany, 2013.
6. Backe, H.; Lauth, W.; Block, M.; Laatiaoui, M. Prospects for laser spectroscopy, ion chemistry and mobility measurements of superheavy elements in buffer-gas traps. *Nucl. Phys. A* **2015**, *944*, 492–517.
7. Sato, T.; Asai, M.; Borschevsky, A.; Stora, T.; Sato, N.; Kaneya, Y.; Tsukada, K.; Düllmann, C.E.; Eberhardt, K.; Eliav, E.; et al. Measurement of the first ionization potential of lawrencium, element 103. *Nature* **2015**, *520*, 209–211.
8. Sato, T.K.; Asai, M.; Borschevsky, A.; Beerwerth, R.; Kaneya, Y.; Makii, H.; Mitsukai, A.; Nagame, Y.; Osa, A.; Toyoshima, A.; et al. First ionization potentials of Fm, Md, No, and Lr: Verification of filling-up of 5f electrons and confirmation of the actinide series. *J. Am. Chem. Soc.* **2018**, *140*, 14609–14613.
9. Laatiaoui, M.; Lauth, W.; Backe, H.; Block, M.; Ackermann, D.; Cheal, B.; Chhetri, P.; Düllmann, C.E.; Van Duppen, P.; Even, J.; et al. Atom-at-a-time laser resonance ionization spectroscopy of nobelium. *Nature* **2016**, *538*, 495–498.
10. Chhetri, P.; Ackermann, D.; Backe, H.; Block, M.; Cheal, B.; Droese, C.; Düllmann, C.E.; Even, J.; Ferrer, R.; Giacoppo, F.; et al. Precision measurement of the first ionization potential of nobelium. *Phys. Rev. Lett.* **2018**, *120*, 263003.
11. Neugart, R.; Billowes, J.; Bissell, M.; Blaum, K.; Cheal, B.; Flanagan, K.; Neyens, G.; Nörtershäuser, W.; Yordanov, D. Collinear laser spectroscopy at ISOLDE: New methods and highlights. *J. Phys. G Nucl. Part. Phys.* **2017**, *44*, 064002.
12. Fedosseev, V.; Chrysalidis, K.; Goodacre, T.D.; Marsh, B.; Rothe, S.; Seiffert, C.; Wendt, K. Ion beam production and study of radioactive isotopes with the laser ion source at ISOLDE. *J. Phys. G Nucl. Part. Phys.* **2017**, *44*, 084006.
13. Lautenschläger, F.; Chhetri, P.; Ackermann, D.; Backe, H.; Block, M.; Cheal, B.; Clark, A.; Droese, C.; Ferrer, R.; Giacoppo, F.; et al. Developments for resonance ionization laser spectroscopy of the heaviest elements at SHIP. *Nucl. Instrum. Methods Phys. Res. Sect. B Beam Interact. Mater. At.* **2016**, *383*, 115–122.
14. Backe, H.; Kunz, P.; Lauth, W.; Dretzke, A.; Horn, R.; Kolb, T.; Laatiaoui, M.; Sewtz, M.; Ackermann, D.; Block, M.; et al. Towards optical spectroscopy of the element nobelium ($Z = 102$) in a buffer gas cell. *Eur. Phys. J. D* **2007**, *45*, 99–106.
15. Raeder, S.; Ackermann, D.; Backe, H.; Beerwerth, R.; Berengut, J.; Block, M.; Borschevsky, A.; Cheal, B.; Chhetri, P.; Düllmann, C.E.; et al. Probing sizes and shapes of nobelium isotopes by laser spectroscopy. *Phys. Rev. Lett.* **2018**, *120*, 232503.
16. Münzenberg, G.; Faust, W.; Hofmann, S.; Armbruster, P.; Güttner, K.; Ewald, H. The velocity filter SHIP, a separator of unslowed heavy ion fusion products. *Nucl. Instrum. Methods* **1979**, *161*, 65–82.
17. Murböck, T.; Raeder, S.; Chhetri, P.; Diaz, K.; Laatiaoui, M.; Giacoppo, F.; Block, M. Filament studies for laser spectroscopy on lawrencium. *Hyperfine Interact.* **2020**, *241*, 1–9.
18. Laatiaoui, M.; Backe, H.; Block, M.; Chhetri, P.; Lautenschläger, F.; Lauth, W.; Walther, T. Perspectives for laser spectroscopy of the element nobelium. *Hyperfine Interact.* **2014**, *227*, 69–75.
19. Oganessian, Y.T.; Utyonkov, V.; Lobanov, Y.V.; Abdullin, F.S.; Polyakov, A.; Shirokovsky, I.; Tsyganov, Y.S.; Mezentssev, A.; Iliev, S.; Subbotin, V.; et al. Measurements of cross sections for the fusion-evaporation reactions $^{204,206,207,208}\text{Pb} + ^{48}\text{Ca}$ and $^{207}\text{Pb} + ^{34}\text{S}$: Decay properties of the even-even nuclides ^{238}Cf and ^{250}No . *Phys. Rev. C* **2001**, *64*, 054606.
20. Gäggeler, H.; Jost, D.; Türler, A.; Armbruster, P.; Brüchle, W.; Folger, H.; Heßberger, F.; Hofmann, S.; Münzenberg, G.; Ninov, V.; et al. Cold fusion reactions with ^{48}Ca . *Nucl. Phys. A* **1989**, *502*, 561–570.
21. Zou, Y.; Fischer, C.F. Resonance transition energies and oscillator strengths in lutetium and lawrencium. *Phys. Rev. Lett.* **2002**, *88*, 183001.
22. Borschevsky, A.; Eliav, E.; Vilkas, M.; Ishikawa, Y.; Kaldor, U. Transition energies of atomic lawrencium. *Eur. Phys. J. D* **2007**, *45*, 115–119.
23. Fritzsche, S.; Dong, C.; Koike, F.; Uvarov, A. The low-lying level structure of atomic lawrencium ($Z = 103$): Energies and absorption rates. *Eur. Phys. J. D* **2007**, *45*, 107–113.
24. Dzuba, V.; Safronova, M.; Safronova, U. Atomic properties of superheavy elements No, Lr, and Rf. *Phys. Rev. A* **2014**, *90*, 012504.
25. Kahl, E.; Raeder, S.; Eliav, E.; Borschevsky, A.; Berengut, J. Ab initio calculations of the spectrum of lawrencium. *Phys. Rev. A* **2021**, *104*, 052810.
26. Laatiaoui, M.; Backe, H.; Habs, D.; Kunz, P.; Lauth, W.; Sewtz, M. Low-field mobilities of rare-earth metals. *Eur. Phys. J. D* **2012**, *66*, 1–5.
27. Raeder, S.; Block, M.; Chhetri, P.; Ferrer, R.; Kraemer, S.; Kron, T.; Laatiaoui, M.; Nothhelfer, S.; Schneider, F.; Van Duppen, P.; et al. A gas-jet apparatus for high-resolution laser spectroscopy on the heaviest elements at SHIP. *Nucl. Instrum. Methods Phys. Res. Sect. B Beam Interact. Mater. At.* **2020**, *463*, 272–276.
28. Kaleja, O.; Anđelić, B.; Blaum, K.; Block, M.; Chhetri, P.; Droese, C.; Düllmann, C.E.; Eibach, M.; Eliseev, S.; Even, J.; et al. The performance of the cryogenic buffer-gas stopping cell of SHIPTRAP. *Nucl. Instrum. Methods Phys. Res. Sect. B Beam Interact. Mater. At.* **2020**, *463*, 280–285.
29. Barzakh, A.; Chubukov, I.Y.; Fedorov, D.; Moroz, F.; Panteleev, V.; Seliverstov, M.; Volkov, Y.M. Isotope shift and hyperfine structure measurements for ^{155}Yb by laser ion source technique. *Eur. Phys. J. A Hadron. Nucl.* **1998**, *1*, 3–5.

30. Sprouse, G.; Das, J.; Lauritsen, T.; Schecker, J.; Berger, A.; Billowes, J.; Holbrow, C.; Mahnke, H.E.; Rolston, S. Laser spectroscopy of light Yb isotopes on-line in a cooled gas cell. *Phys. Rev. Lett.* **1989**, *63*, 1463.
31. Barzakh, A.; Fedorov, D.; Panteleev, V.; Seliverstov, M.; Volkov, Y.M. Measurements of charge radii and electromagnetic moments of nuclei far from stability by photoionization spectroscopy in a laser ion source. In *AIP Conference Proceedings*; American Institute of Physics: Melville, NY, USA, 2002; Volume 610, pp. 915–919.
32. Das, D.; Barthwal, S.; Banerjee, A.; Natarajan, V. Absolute frequency measurements in Yb with 0.08 ppb uncertainty: Isotope shifts and hyperfine structure in the 399-nm $^1S_0 \rightarrow ^1P_1$ line. *Phys. Rev. A* **2005**, *72*, 032506.